






Paper Type: Original Article

Thermodynamic Simulations of Exergy Efficiency in Organic Rankine Cycle (ORC) Based on Exergy System

Imoh Ime Ekanem¹ , Enefiok Okon Usungurua² , Aniekan Essienubong Ikpe^{1,*} 

¹ Department of Mechanical Engineering, Akwa Ibom State Polytechnic, Ikot Osurua, Ikot Ekpene, Nigeria; imoh.ekanem@akwaibompoly.edu.ng; aniekan.ikpe@akwaibompoly.edu.ng.

² Department of Mechanical Engineering, Federal University of Technology, Ikot Abasi, Nigeria; eneusungurua@futia.edu.ng.

Citation:

Received: 05 March 2024

Revised: 20 June 2024

Accepted: 15 October 2024

Ekanem, I. I., Usungurua, E. O., & Ikpe, A. E. (2024). Thermodynamic simulations of exergy efficiency in organic Rankine cycle (ORC) based on exergy system. *Annals of process engineering and management*, 1(1), 1-25.

Abstract

Exergy analysis in a biomass-powered cycle is vital, especially when involving thermo-chemical conversion technologies like gasification and Pyrolysis. These involve complex analyses and have comparative advantages to combustion techniques in power generation. This study conducted a thermodynamic simulation of the exergy efficiency of a novel Organic Rankine Cycle (ORC) with turbine bleeding for tri-generation to ascertain the optimal intrinsic values and their real-time boundaries for efficient power output. The study employed a replication method with a developed soft template written source code in Engineering Equation Solver (EES) compared to inconsistent and untactful productivity identified with energy-sapping blue-collar analysis of the system that was invoked hitherto, using three working fluids: R245fa, R1234yf and R1234ze bounded by environmental and safety standards, and valuable temperatures, pressures and mass flow rates. The results showed that exergy efficiencies for R1234ze, R245fa and R1234yf were recorded as 29.61%, 28.34% and 22.32% respectively. In contrast, the generic ORC without turbine bleeding with the same configuration had corresponding respective efficiencies of 13.25%, 15.33% and 14.06%, which were relatively low, particularly with respect to ORC system without cooling, and having respective efficiency improvement of 16.36%, 13.0% and 8.26%. Additionally, the total output power was 201.0KW for R245fa, 162.5 KW for R1243ze and 131.7 KW for R1234yf having Turbine Inlet Temperatures (TITs) spread between 90-120°C in general. Based on the evaluated thermodynamic properties and their output, especially enthalpy, entropy and exergy destruction, R234fa is given preference, with the highest overall efficiency, followed by 1234ze then 1234fy in that order. The designed ORC system has the potential for medium temperature relevance with agricultural wastes and for biomass energy utilisation with reduced vent gases compared to most ORC systems used for low-grade heat sources such as geothermal and solar applications, which are wasted as thermal pollution.

Keywords: Gasification, Pyrolysis, Combustion, Thermodynamic simulation, Exergy efficiency.

1 | Introduction

The increasing energy crises and rapid industrialization of the world have made global warming and other environmental deteriorations foreseeable [1]. Meanwhile, fossil fuels are particularly important in the overall energy sector. Fossil fuels remain dominant in the global energy industry, valued at approximately 1.5 trillion dollars. Concerning the World Energy Outlook (WEO) 2007, fossil fuel energy will continue to be the primary

 Corresponding Author: aniekan.ikpe@akwaibompoly.edu.ng



 Licensee System Analytics. This article is an open-access article distributed under the terms and conditions of the Creative Commons Attribution (CC BY) license (<http://creativecommons.org/licenses/by/4.0>).

energy source, meeting approximately 84% of demand in 2030 [2]. However, using fossil fuels to generate energy has a significant environmental impact. Therefore, improved conversion efficiency is critical to comprehend the potential of our resources completely [3].

Hence, this study tackles thermodynamic simulations of exergy efficiency in a biomass-fired Organic Rankine Cycle (ORC) with turbine bleeding for tri-generation using a developed soft template written source code in Engineering Equation Solver (EES) to determine the optimal operating conditions for maximum functional work output for the considered refrigerants. This is novel against the labour intensiveness, and inefficiencies witnessed in manual and physical investigations that were invoked previously. Additionally, most ORC systems are used for low-grade heat sources such as geothermal and solar applications; hence, this study also attempts to design an ORC system for medium temperature to be used with agricultural wastes and for biomass energy utilisation. In the quest to tackle this and future energy demand, while reducing greenhouse gas emissions and dependence on fossil fuels, improvement of energy systems is inevitable. Studies show that more than 50% of the total heat generated in the industry is considered low-grade heat and is wasted as thermal pollution. In contrast, the ORC and Regenerative Organic Rankine Cycle (RORC) are beneficial in this scenario [4], [5].

In the world, energy demonstrates itself in a multiplicity of forms, each having its own conventional characteristics and qualities [6]. The historical suitability of energy quality can be identified while carrying out mechanical work. Consequently, the ability to affect change or perform productive labour describes today's energy value [7]. Natural observations show that different types of energy have different abilities to convert into other forms. Furthermore, this capability depends on the system's configuration, state characteristics, and environment. It is only rational for the energy quality index to identify the transformability of a particular type of energy to the environment, a reality that the universal law of energy conservation overlooks. Nevertheless, the second law of thermodynamics, which establishes some limitations on the direction and magnitude of energy transformations, bridges this gap in understanding energy transformations [6]–[8].

Ahmadi et al. [9] said that the ORC is considered to be a very successful technology for recovering heat and producing electricity at low and medium temperatures (300–450 °C). One significant advantage of ORC is its versatility in applications such as biomass combustion, geothermal systems, and solar desalination systems. Additionally, it is particularly valuable when dealing with low-temperature exhaust gases from gas turbines. ORC's high dependability and versatility make it particularly desirable [10]–[17]. Quoilin et al. [18] focused on optimizing the thermodynamics and economics of a small-scale ORC used in waste heat recovery. Sun et al. [14] improved the efficiency of an ORC by optimizing two goal functions. It was determined that the controlled and uncontrolled variables are linear when optimizing the total net power generation and a quadratic relationship when maximizing the system's thermal efficiency. In addition, other strategies are available to enhance an ORC system's performance. These approaches include optimizing system operation, integrating feed-water heating, merging other system techniques, and integrating turbine bleeding and regeneration [19].

In this way, Jin et al. [20] and Desai and Bandyopadhyay [21] have revealed that the thermal efficiency of an ORC can be meaningfully enhanced by incorporating turbine bleeding and regeneration and turbine bleeding for tri-generation, as also considered in this study. Notwithstanding the numerous investigations regarding ORC, like system performance modelling, selection of an appropriate working fluid, optimization, and so on, detailed energy and exergy analysis of the elementary and diverse modified ORC cycles were hardly established [22].

Exergy measures a thermodynamic process's maximum usable work output or minimal needed work input under a defined system and surrounding circumstances [23]. Exergy efficiency illustrates how far the efficiency of a conversion process is from its theoretical maximum. The second law of thermodynamics analysis and exergy destruction first appeared in ORC, and the combined cycle did not last long afterwards. However, the combined cycle exergy-based study has recently added a significant addition. Many researchers, like Kotas [24] and Moran et al. [25], carried out exergy analysis and found exergy losses in every component for

the combined cycles. Long et al. [26] conducted internal and external exergy analyses to institutionalize the system's response to the working fluids. To determine this influence, a simpler internal exergy efficiency model is given. The calculations revealed that thermo-physical parameters of working fluids have minimal influence on internal exergy efficiency, but they are crucial in determining peripheral exergy efficiency.

Energy analysis is the most frequently adopted technique for estimating energy transformation procedures. However, it has some characteristic restrictions, such as not categorizing the energy quality and irreversibility of procedures through the system. On the contrary, exergy analysis will categorize the work potential of the systems. It offers a more accurate interpretation of various components and procedures for evaluating efficiency and exergy losses to trace the primary margins for enhancements [27]–[31].

Therefore, this paper focuses on building a hypothetical framework for the exergy analysis of the ORC, which can be used to calculate the exergy efficiencies and exergy destruction in each component and the overall system. In addition to the basic ORC, a modified ORC with regeneration and turbine bleeding is investigated to improve the system performance. This study presents thermodynamic assumptions for the three refrigerants: R245fa, R1234yf and R1234ze employed in the simulations, their physical properties as well as the environmental and safety indices of the refrigerants. Results of thermodynamic simulations of the overall system, cycle performance at standard conditions, exergy destruction and output, and the effect of turbine inlet pressure on exergy efficiency and turbine output are equally presented.

1.1 | Environmental Impact Considerations for Organic Rankine Cycle Working Fluid Selection

The working fluid used significantly impacts the system's performance and functioning. Fluids used in these systems can be characterized as isentropic, dry, or wet, depending on whether the slope of the saturation curve in the T-S diagram is infinite, positive, or negative [32]. Wet fluid is usually incompatible with systems; the ORC accumulation of liquid droplets on the turbine blade causes erosion, so it must be superheated. The volumetric expander, on the other hand [33], at the inlet taking a high liquid fraction such as screw expander and scroll expander, shows the advantage which allows the design of wet cycles [34]. In other words, wet fluid is projected to be a promising fluid for ORCs that do not require superheating. Kuo et al. [35] claimed no physical attribute can be utilized as the only indication for quantitatively screening the working fluid. As a result, a non-dimensional figure of merit was developed. Hung [36] showed that specific heat, latent heat, and the slope of the saturation vapour curve are all essential physical properties to consider while screening the working fluid. Tchanche et al. [37] preferred working fluids with many latent and specific heat. According to Yamamoto et al. [38], low latent heat is preferable. However, high latent heat and low liquid-specific heat are ideal. Generally, for temperatures between 380K and 430K, it was found that R123, R245a and R245fa are better working fluids, whereas for the less than 380K application, Isobutane is more appropriate. In medium-grade heat sources like in biomass applications, most fluids for low-temperature sources cannot be adopted; this is because of high vapour pressure at these condensation temperatures [39]–[42].

1.2 | Biomass-based Energy Conversion Systems

Several studies have been done to maximize alternative energy sources due to the world's concern about the depletion of fossil fuels and the effects of climate change. According to the WEO 2010 [2] published by the International Energy Agency (IEA), fossil fuels account for over 81% of the world's energy consumption. Among sustainable and renewable resources, biomass accounts for the most, with 10%, reflecting contemporary and historical usage. The IEA is projecting that biomass will continue to be the most prominent renewable energy source by the year 2035, based on the present energy scenario. As a renewable energy source, biomass is environmentally friendly and does not contribute to soaring CO₂ levels as it captures ambient CO₂ gas during photosynthesis. Nigeria's plantation and agricultural output dwarfs its biomass

consumption as an energy fuel. Typically, the most efficient method of producing electricity from biomass on a large scale is to combine it with coal, which may increase efficiency to 45%. On the other hand, a solid biomass-fired plant uses a steam turbine (Rankine cycle) to produce steam by burning the fuel. Working fluids with a lower ebullition (critical temperature) and a larger molecular mass are better suited for usage in small and medium systems [43], [44].

1.3 | The Concept of Tri-generation and Multi-generation Energy Systems

Tri-generation is a thermal system that utilizes the heat loss from a steam turbine to generate power, cooling, and distilled water simultaneously. This system operates without additional fuel and is highly regarded for its environmental friendliness when operated by solar energy. The waste heat generated by the primary mover in the tri-generation system is utilized to enhance the system's efficiency, achieving a level of 85% [45]. Solar thermal power generation is receiving significant interest and is widely used in commercial applications. The effectiveness of these devices has been the subject of research [46]. Nafey et al. [47] compared three different types of thermal energy collectors: a parabolic trough, a flat plate, and a compound parabolic concentrator—that might power an ORC. For the analysis, they used MATLAB/SimuLink code. Reverse Osmosis (RO) desalination was powered by the electrical power generated by the ORC. The results indicated that Toluene, Butane, Hexane, parabolic trough Collector, flat plate Collector, and compound parabolic concentrator all functioned well. Using compound parabolic concentrators as collectors and HCFC-123 as the working fluid, Al-Sulaiman et al. [4] performed a computational study that simulated the solar ORC. Thermodynamic modelling and parametric evaluation for three electrical power plants were part of the study, which also looked into the techniques to improve efficiency in tri-generation scenarios. Solar trigeneration, biomass trigeneration, and solid oxide fuel cell trigeneration were the facilities being considered. With a tri-generation efficiency of 90%, the solar and biomass systems outperformed all others, while the SOFC-tri-generation system demonstrated the highest electrical efficiency. The facilities that produced the most CO₂ emissions per megawatt-hour used biomass and SOFC trigeneration.

1.4 | Organic Rankine Cycles and Its Multiple Applications

Zahedi et al. [48] said that the ORC subsystem and steam cycle could help make electricity much better. According to Jouhara et al. [49], ORC has an advantage over the Kalina cycle in the low-medium range. The Kalina cycle provides superior results in medium-high grades. For waste heat recovery that is not constant, a double ORC was investigated by Wang et al. [50]. At a particular Pinch Point Temperature Difference (PPTD), the effect of heat source outlet temperature on net power production, mass flow rate, power consumption, expander outlet temperature, cycle irreversibility, thermal efficiency, and exergy efficiency was investigated. Also, Li et al. [51] noted that using hybrid ORC system technologies can obtain the highest performance in the presence of variable heat sources. Kaska [52] showed how the system's energy and exergy efficiencies changed with subcooling, superheating, and evaporator/condenser pressures. 10.2%, 48.5%, and 8.8%, 42.2% are energy and exergy efficiencies, respectively, for two separate real scenarios, according to the research. Subcomponent exergy destruction was also measured. Baroutaji et al. [53] proposed an ORC for generating electricity from the Proton-Exchange Membrane Fuel Cell's waste heat. Based on exergy recovery, Wu et al. [54] presented an evaporator model in ORC that recovers waste heat. The research also provided a novel technique that may be used to design evaporators for waste heat recovery-based power production. Karellas et al. [55] suggested waste heat recovery extract energy from cement factory exhaust fumes. Waste heat recovery has been studied using the water-steam cycle and ORC. The two waste heat recovery methods were compared, and their energy and exergy evaluations were reported.

Several researchers have also looked at regenerative ORC. Laouid et al. [56] took two scenarios for the optimization: one included the combination of exergy efficiency and the cost of producing electricity, and the other involved net power output and the cost of producing electricity. Based on the findings, they said that ORC layouts may be more desirable for achieving the goals of net power output and electricity production. Additionally, the RORC configurations had the lowest electricity costs, followed by the basic ORC. However,

research revealed that wet fluids in the RORC arrangement worked better. Mago et al. [57] investigated using dry organic fluids in regenerative ORCs to transform waste low-grade heat energy sources into proper energy forms. Using four dry organic working fluids: R245ca, R113, isobutene, and R123, they examined basic ORC and regenerative ORC, utilizing both first and second law analysis for different temperatures and pressures as a reference. The regenerative solar ORC was improved by Hajabdollahi et al. [58]. They compared R245fa with R123 using design factors such as evaporator pressure, refrigerant mass flow rate, condenser pressure, number of solar panels, regenerator effectiveness, and storage capacity. Wang et al. [59] considered flat-plate solar collectors and thermal storage devices while modelling a regenerative ORC for using solar energy throughout a low-temperature range. They demonstrated that, given actual restrictions, system performance might be enhanced by raising turbine intake pressure and temperature or reducing turbine backpressure, as well as with a saturated vapour input and employing a higher Turbine Inlet Temperature (TIT). Darvish et al. [60] used nine working fluids to model the regenerative ORC's thermodynamic performance to identify appropriate organic working fluids. Roy et al. [61] investigated regenerative ORC when the pressure is constant at 250 MPa, utilizing R123 and R134a during superheating based on optimization. Under continuous heat source conditions in waste heat recovery, thermo-economic optimization of basic ORC with regenerative ORC for multiple uses was assessed by Imran et al. [62]. Bernardo et al. [63] examined the feasibility of ORC in the ceramic industry and found that electricity from the ORC system saved around 237 MWh of primary energy, which is equivalent to 31 tons per year of CO₂ emissions.

A tri-generation system can employ various primary energy sources, including internal combustion engines, gas turbines, fuel cells, Rankine cycles, and stirring engines. The Rankine cycle is a highly prospective technology for power generation. Two distinct variations of the Rankine cycle efficiently transform heat energy into usable mechanical work. There are two types of cycles: 1) the steam Rankine cycle, which employs water as a refrigerant, and 2) the ORC, which utilizes organic fluids as refrigerants. The ORC has gained increased attention for domestic uses due to its favourable characteristics of low pressure and temperature productivity [64]–[66].

2 | Materials and Methods

The materials used in this study were: gasifier, cyclone, evaporator, turbine, domestic water heater, heat exchanger, condenser, centrifugal pump, expansion valve and refrigerants; R245fa, R1234yf and R1234ze.

2.1 | Experimental Procedures

A novel biomass-based tri-generation system with a gasifier was analysed. Then, the hot gas was allowed to pass through a cyclone where any trace of ash was settled down. After that, it went through an evaporator, which acted as the heat exchanger and part of the refrigerant bled for expansion while part was allowed to expand entirely to condenser pressure. The refrigerant stream was condensed and pumped through a heat exchanger, increasing its energy level before entering the evaporator to start the cycle again. Afterwards, equilibrium energy models for the gasification process were developed assuming thermodynamic equilibrium reactions and the Pyrolysis product combusted and reached equilibrium on the reaction zone before leaving the gasifier. Equilibrium constants and energy balance were determined for the novel ORC, considering enthalpy and mass flows. Finally, the exergy balance and efficiencies were determined along with the overall performance analysis and calculations.

2.2 | Innovative Biomass-fired Organic Rankine Cycle with Turbine Bleeding for Tri-generation Energy System

The innovative biomass-based tri-generation system consisted of a biomass gasifier which powered the system and replaced the traditional topping cycle. Biomass was partly combusted with a limited supply of air in a gasifier. The hot gas was allowed to pass through the cyclone, where any trace of ash was settled down. The resulting hot gas was passed to an evaporator as a heat exchanger to power the novel ORC. The system

received heat from the evaporator at gasifier temperature, and the pump pressure expanded in a turbine, producing electricity. A part of the refrigerant was bled after expansion, while the remaining part expanded ultimately to condenser pressure. The bled refrigerant vapour existed at a high temperature and pressure, which made it suitable for condensation and evaporation. However, following the high pressure after part expansion in the turbine, an expansion valve was provided that reduced the pressure before condensation. Another expansion valve was provided, further reducing the pressure before the expansion, which brought cooling. After interacting with the heat exchanger, the refrigerant stream that left the evaporator added to the fully expanded vapour. This stream was condensed and pumped through a heat exchanger that increased the energy level before it entered the evaporator to start the cycle again. The schematic diagram is shown in Fig. 1. The analysis presented the temperature profile at all state points, input and output enthalpies, exergy flows, exergy destruction and efficiencies, and environmental sustainability. The relevant energy balances and governing equations developed were described as well.

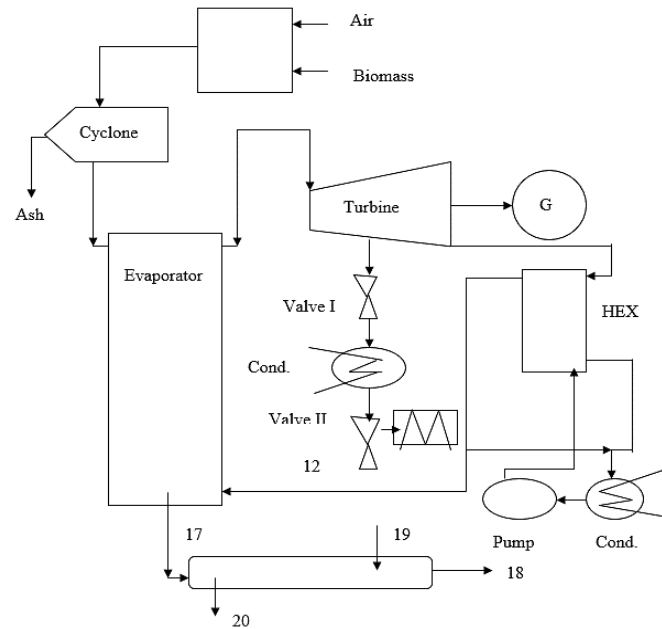


Fig. 1. Biomass-fired organic Rankine cycle-based energy system.

2.3 | Equilibrium Energy Models for the Gasification Process

The model for the gasifier assumed the reactions to be in thermodynamic equilibrium. The Pyrolysis product burned and achieved equilibrium in the reaction zone before leaving the gasifier. Based on these conditions, an equilibrium model was in the downdraft gasifier with the following reactions [46]:



The shift reaction was obtained by the combination of Eqs. (1) and (2)



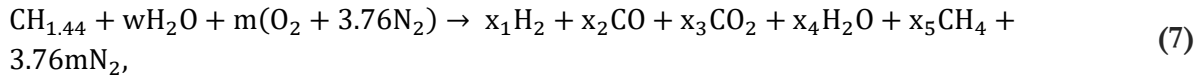
By considering Eqs. (2) and (3), the equilibrium constant for the reactions was expressed as

$$K_1 = \frac{P_{\text{CH}_4}}{(P_{\text{H}_2})^2}, \quad (5)$$

and

$$K_2 = \frac{P_{CH_4} P_{H_2}}{P_{CO} P_{H_2O}} \quad (6)$$

Following the reactions above, the global gasification reaction for wood, considered in this study, was expressed as [46]:



In Eq. (7), w denoted the amount of water per Kmol of wood, m denoted the amount of Oxygen per Kmol of wood, while the x_1, x_2, x_3, x_4 and x_5 represented the coefficients of the product. The moisture content of the wood was related to the amount of water per Kmol of wood with the relationship:

$$MC = \frac{\text{mass of water}}{\text{mass of wet biomass}} \times 100. \quad (8)$$

$$MC = \frac{18w}{24 + 18w}. \quad (9)$$

Accordingly, the amount of water per Kmol of wood was obtained from Eq. (9) as follows:

$$MC = \frac{24MC}{18(1 - MC)}. \quad (10)$$

2.4 | Determination of Product Coefficients

From the gasification reactions in Eq. (7), there were six unknowns; x_1, x_2, x_3, x_4, x_5 and m . Therefore, the equations must suffice to obtain these unknown parameters. This was obtained by using constituents (Carbon, Hydrogen and Oxygen) balance, two equilibrium equations for equilibrium constants, and the reaction of enthalpy of combustion involving ideal enthalpy values.

For elemental balances

$$\text{Carbon balance: } 1 = x_2 + x_3 + x_5. \quad (11)$$

$$\text{Hydrogen balance: } 2w + 1.44 = 2x_1 + 2x_4 + 4x_5. \quad (12)$$

Eq. (12) was reduced to:

$$w + 0.72 = x_1 + x_4 + 2x_5. \quad (13)$$

$$\text{Oxygen balance: } w + 0.66 + 2m = x_2 + 2x_3 + x_4. \quad (14)$$

From Eq. (5), the equilibrium constant for methane formation was obtained as follows.

$$K_1 = \frac{x_5}{x_1^2} \rightarrow K_1 x_1^2 - x_5 = 0. \quad (15)$$

Similarly, from Eq. (6), the equilibrium constant from the shift reaction was expressed as

$$K_2 = \frac{x_1 x_3}{x_2 x_4} \rightarrow K_1 x_2 x_4 - x_1 x_3 = 0. \quad (16)$$

Eqs. (4)-(8) constitute five of the required six equations necessary to determine the product coefficients.

The heat balance equation for the gasification process under adiabatic conditions was presented thus;

$$H^0_{f_{wood}} + w(H^0_{f_{H_2O}} + H_{vap}) + mH^0_{f_{O_2}} + 3.76mH^0_{f_{N_2}} = x_1H^0_{f_{H_2}} + x_2H^0_{f_{CO_2}} + x_4H^0_{f_{H_2O}} + x_1H^0_{f_{effu}} + (T_{gasif} - T_{ref})(x_1C_{P_{H_2}} + x_2C_{P_{CO}} + x_3C_{P_{CO_2}} + x_4C_{P_{H_2O}} + x_5C_{P_{CH_4}} + 3.76mC_{P_{N_2}}). \quad (17)$$

The enthalpy of Hydrogen, Nitrogen and Oxygen formation is zero at ambient temperature. Consequently, Eq. (9) was reduced to:

$$H^0_{f_{wood}} + w(H^0_{f_{H_2O}} + H_{vap}) = x_2H^0_{f_{CO}} + x_3H^0_{f_{CO_2}} + x_4H^0_{f_{H_2O(ref)}} + x_5H^0_{f_{CH_4}} + (T_{gasif} - T_{ref})(x_1C_{P_{H_2}} + x_2C_{P_{CO}} + x_3C_{P_{CO_2}} + x_4C_{P_{H_2O}} + x_5C_{P_{CH_4}} + 3.76mC_{P_{N_2}}), \quad (18)$$

where $H^0_{f_{wood}}$, $H^0_{f_{H_2O}}$, $H^0_{f_{H_2O(vap)}}$, $H^0_{f_{CO}}$, $H^0_{f_{CO_2}}$ and $H^0_{f_{CH_4}}$ respectively denoted heat of formation of wood biomass, liquid water, water vapour, Carbon (II) oxide, Carbon (IV) oxide and Methane. T_{gasif} and T_{ref} respectively denoted gasification temperature and reference or ambient temperature, whereas C_{P_i} denoted specific heats of gas products, and i represented H_2 , CO , CO_2 , H_2O , CH_4 and N_2 .

To determine values for the equilibrium constants, the following relation was applied [67]:

$$-RT\ln(K) = \Delta G^0. \quad (19)$$

where ΔG^0 is the standard Gibbs's function of formation. The dependence of ΔG^0 on temperature can be written as follows:

$$\frac{d(\Delta G^0/RT)}{dT} = \frac{-\Delta H^0}{RT^2}. \quad (20)$$

$$\therefore \frac{\Delta G^0}{RT} = -\ln(K). \quad (21)$$

Substituting Eq. (13) in Eq. (12) we had:

$$\frac{d(\ln [K])}{dT} = \frac{\Delta H^0}{RT^2}. \quad (22)$$

Eq. (14) expressed the effect of temperature in the equilibrium constant. It followed that for an exothermic reaction (ΔG^0 is negative), the equilibrium constant K will be reduced when temperature increases. However, K increased with decrease T for an endothermic reaction. Integrating Eq. (14):

$$\ln(K) = \int \frac{\Delta H^0}{RT^2} + \varepsilon \quad (23)$$

where ε is the constant of integration and from Eq. (15), ΔH^0 was given thus [67]:

$$\frac{\Delta H^0}{R} = \frac{J}{R} + (\Delta A)T + \frac{\Delta B T^2}{2} + \frac{\Delta C T^3}{3} - \frac{\Delta D}{T}. \quad (24)$$

here J is a constant, and ΔA , ΔB , ΔC and ΔD are coefficients for determining specific heat.

Substituting Eq. (15) into Eq. (16) integrating we had:

$$\ln(K) = \frac{-J}{RT} + \Delta A \ln T + \frac{\Delta B}{2} T + \frac{\Delta C}{6} T^2 + \frac{\Delta D}{2T^2}. \quad (25)$$

From Eq. (11), $\Delta G^\circ = -RT \ln(K)$ and multiplying Eq. (17) by $-RT$ gave;

$$\Delta G^\circ = J - RT(\Delta A \ln(T) + \frac{\Delta B}{2} T + \frac{\Delta C}{6} T^2 + \frac{\Delta D}{2T^2}) + I, \quad (26)$$

where I is irreversibility and Eqs. (24)-(26) were used to determine the equilibrium constants at any reaction temperature.

Therefore, the determination of equilibrium constants aided the solving of Eqs. (1) and (2), Eqs. (4)-(6) and Eq. (8), where the gasification temperature as well as the mole constituents of the product gas were determined.

2.5 | Energy Balance for the Novel Organic Rankine Cycle

The energy balance for each component of the novel ORC was presented considering both enthalpy and mass flows as follows:

Evaporator energy balance

The energy balance for the evaporator was a function of the state properties at points 1, 12, 16, and 17, and was represented as

$$m_1 h_1 + m_{12} h_{12} = m_{16} h_{16} + m_{17} h_{17}. \quad (27)$$

The temperature leaving the evaporator to the domestic water heater was estimated with the following relationship:

$$T_{17} = T_{12} + T_{pp}, \quad (28)$$

where T_{pp} represented evaporator pinch point temperature.

Domestic water heater energy balance

Similarly, the energy balance for the domestic water heater was expressed with the relationship:

$$m_{17} h_{17} + m_{19} h_{19} = m_{18} h_{18} + m_{20} h_{20}. \quad (29)$$

Organic Rankine cycle turbine energy balance

The state points encompassing the gas turbine were points 1, 2, and 3 and the work output W_{GT} . From Eq. (19), the property values of state 1 were evaluated, especially the entropy at points 2 and 3. The expansion process was isentropic. Consequently,

$$s_1 = s_2 = s_3. \quad (30)$$

The energy balance for the turbine was expressed as [32], [33], [68]:

$$h_1 = h_2 + (1 - x)(h_2 - h_3) + W_{GT}, \quad (31)$$

where the fraction of bled steam from the system at point 2 was denoted by x . Due to identical entropy values at points 1, 2 and 3, the enthalpy at point 2 was obtained corresponding to p_2 , while that at point 3 was obtained at a pressure which corresponded to p_3 . When considering turbine isentropic efficiency, h_{2a} and h_{3a} were obtained from the relations:

$$\eta_{GT} = \frac{h_2 - h_{2a}}{h_1 - h_2}. \quad (32)$$

$$\eta_{GT2} = \frac{h_2 - h_{3a}}{h_2 - h_3}. \quad (33)$$

The net work done by the turbine in terms of the pump work was expressed thus;

$$W_{GT} = (h_1 - h_2) + (1 - x)(h_2 - h_3). \quad (34)$$

While the thermal efficiency of the cycle was expressed using the relation as follows:

$$\eta_{Therm} = \frac{W_{GT}}{h_{13} - h_{14}} = \frac{(h_1 - h_2) + (1 - x)(h_2 - h_3)}{h_{13} - h_{14}}. \quad (35)$$

Heat exchanger energy balance

The heat exchanger was enclosed by state points 3, 8, 11 and 12. Energy balance for the heat exchanger in terms of enthalpy or temperature was used in computing state values at point 8 as presented;

$$h_3 - h_{11} = h_{12} - h_8. \quad (36)$$

The effectiveness of the heat exchanger was expressed in terms of the enthalpies [32], [33];

$$\varepsilon = \frac{h_3 - h_8}{h_3 - h_{11}}. \quad (37)$$

$$\varepsilon = \frac{h_{12} - h_{11}}{h_3 - h_{11}}. \quad (38)$$

$$\text{Valve I (2,4): } h_2 = h_4. \quad (39)$$

$$\text{Condenser (4,5): } h_4 = Q_{cond} + h_5. \quad (40)$$

$$\text{Valve II (5,6): } h_5 = h_6. \quad (41)$$

$$\text{Evaporator (6,7): } h_6 = Q_{evap} + h_7. \quad (42)$$

$$\text{Condenser (9,10): } h_9 = Q_{cond} + h_{10}. \quad (43)$$

Pump energy balance (10, 11)

The energy balance for the pump was expressed by the relation as presented;

$$h_{10} + W_p = h_{11}, \quad (44)$$

where

$$W_p = v_{f10}(P_{11} - P_{10}). \quad (45)$$

$$\therefore h_{11} = h_{10} + v_{f10}(P_{11} - P_{10}). \quad (46)$$

The pump efficiency was denoted by η_{pump} and since the pump was considered isentropic [33], it followed that the pump efficiency can be expressed thus:

$$\eta_{\text{pump}} = \frac{h_{11} - h_{10}}{h_{11a} - h_{10}}. \quad (47)$$

And the enthalpy at point 11 was obtained by solving for h_{11a} as follows:

$$h_{11a} = \frac{h_{11} - h_{f10}}{\eta_p} + h_{f10}. \quad (48)$$

2.6 | Exergy Modelling

The expression for the exergy balance at various components was presented in line with the general exergy balance for a control volume system [68]. Therefore, the general exergy models for a control volume comprising exergy influx ex_{in} , efflux ex_{out} , heat input Q_{in} and work output W_{out} was expressed under steady-state conditions as

$$\sum ex_{in} + ex_Q = \sum ex_{out} + ex_W + E_D, \quad (49)$$

where E_D was the exergy destruction and where the specific exergy was expressed at a temperature T and pressure P , all referenced at the ambient temperature T_0 and pressure P_0 as followed:

$$ex_{in,out} = [(h(T) - h(T_0)) - T_0\{(s(T) - s(T_0))\}]. \quad (50)$$

To properly account for the properties of the system regarding the specific heat capacity at referenced temperature, pressure and other properties, the entropy change was hereby accounted for by employing the thermodynamic first law and necessary simplifications to obtain the expression for the entropy and enthalpy change as shown in [32].

$$\Delta s = c_p \ln \left[\frac{T}{T_0} \right] - R \ln \left[\frac{P}{P_0} \right]. \quad (51)$$

$$\Delta h = c_p \ln [T - T_0]. \quad (52)$$

Substituting these two expressions in *Eq. (42)*, we obtained the term for calculating the physical exergy streams for the four structures as presented.

$$ex_{in,out} = \left\| c_p [T - T_0] - T_0 \left\{ c_p \ln \left[\frac{T}{T_0} \right] - R \ln \left[\frac{P}{P_0} \right] \right\} \right\|. \quad (53)$$

Additionally, the exergy of heat and that of work interaction were expressed as follows.

$$ex_Q = \left[1 - \frac{T_0}{T_Q} \right] Q_{in}. \quad (54)$$

$$ex_W = W = c_p \Delta h. \quad (55)$$

The developed expressions from *Eqs. (49)-(55)* were necessary and sufficient to perform the component exergitic balance as presented.

Evaporator (1, 12, 16, 17)

The exergy balance was presented thus following the general expression in *Eq. (49)*.

$$\dot{E}_{12} + \dot{E}_{16} = \dot{E}_1 + \dot{E}_{17} + \dot{E}_{EVAP}. \quad (56)$$

The exergitic efficiency for the vapour generator was obtained with the expression.

$$\Psi_{VG} = \frac{\dot{E}_1 - \dot{E}_{12}}{\dot{E}_{16} - \dot{E}_{17}}. \quad (57)$$

Turbine (1, 2, 3)

$$\dot{E}_1 = \dot{E}_2 + \dot{E}_3 + \dot{E}_{WT} + \dot{E}_{D,TURB}. \quad (58)$$

$$\Psi_{TURB} = \frac{\dot{E}_{WT}}{\dot{E}_1 - \dot{E}_2 - \dot{E}_3}. \quad (59)$$

Valve I (2, 4)

$$\dot{E}_2 = \dot{E}_4 + \dot{E}_{D,VI}. \quad (60)$$

Condenser (4, 5)

$$\dot{E}_4 = \dot{E}_5 + \dot{E}_{D,COND}. \quad (61)$$

$$\Psi_{COND} = \frac{Q_{COND} \left(1 - \frac{T_0}{T_C}\right)}{\dot{E}_4 - \dot{E}_5}. \quad (62)$$

Valve II (5, 6)

$$\dot{E}_5 = \dot{E}_6 + \dot{E}_{D,II} \quad (63)$$

Evaporator (6, 7)

$$Q_{EVAP} \left(1 - \frac{T_E}{T_\infty}\right) + \dot{E}_6 = \dot{E}_7 + \dot{E}_{D,EVP}. \quad (64)$$

$$\Psi_{EVAP} = \frac{\dot{E}_7 - \dot{E}_6}{Q_{EVAP} \left(1 - \frac{T_E}{T_\infty}\right)}. \quad (65)$$

Heat exchanger (3, 8, 11, 12)

$$\dot{E}_3 + \dot{E}_{11} = \dot{E}_8 + \dot{E}_{12} + \dot{E}_{D,HEX}. \quad (66)$$

$$\Psi_{HEX} = \frac{\dot{E}_{12} - \dot{E}_{11}}{\dot{E}_3 - \dot{E}_8}. \quad (67)$$

Condenser (9, 10)

$$\dot{E}_9 = \dot{E}_{10} + \dot{E}_{D,COND}. \quad (68)$$

$$\Psi_{COND} = \frac{Q_{COND} \left(1 - \frac{T_0}{T_C}\right)}{\dot{E}_9 - \dot{E}_{10}}. \quad (69)$$

Pump (10, 11)

$$\dot{E}_{10} + \dot{E}_{WP} = \dot{E}_{11} + \dot{E}_{D,PUMP}. \quad (70)$$

$$\Psi_{PUMP} = \frac{\dot{E}_{11} - \dot{E}_{10}}{\dot{E}_{WP}}. \quad (71)$$

2.7 | Exergy Efficiency

The exergy efficiency is the parameter that relates the ratio of the exergy of product and exergy of fuel and was expressed for the ORC power generation unit, the CHP unit and the tri-generation system as follows [69].

$$\Psi_{TRIGENERATION} = \frac{\dot{W}_{Net,ORC} + \dot{E}_{Cooling} + \dot{E}_{H_2O}}{\dot{E}_{Biomass}}. \quad (72)$$

$$\Psi_{ORC} = \frac{\dot{W}_{Net,ORC} + \dot{E}_{Cooling}}{\dot{E}_{Biomass}}. \quad (73)$$

The exergy of biomass was defined with the following relationship [69].

$$\dot{E}_{Biomass} = \dot{m}_{Biomass} \beta LHV_{Biomass}. \quad (74)$$

The constant of proportionality β in Eq. (66) is a function of the biomass composition in terms of the number of moles of carbon, Hydrogen and Oxygen and was expressed by

$$\beta = \frac{1.0414 + 0.0177 \left[\frac{H}{C} \right] - 0.3328 \left[\frac{O}{C} \right] \left(1 + 0.0537 \left[\frac{H}{C} \right] \right)}{1 - 0.4021 \left[\frac{O}{C} \right]}. \quad (75)$$

The system environmental impact assessment termed Sustainability Index (SI) was correlated using the quantity of total exergy destruction concerning the quantity of exergy input. Accordingly, the following relationship sufficed for the tri-generation system as presented [70].

$$SI = \frac{\dot{E}_{Biomass}}{\dot{E}_{D,TOTAL}}. \quad (76)$$

By substituting the relevant values for computation of the exergetic SI, the final expression was obtained thus;

$$SI = \frac{\dot{m}_{Biomass} \left[\frac{1.0414 + 0.0177 \left[\frac{H}{C} \right] - 0.3328 \left[\frac{O}{C} \right] \left(1 + 0.0537 \left[\frac{H}{C} \right] \right)}{1 - 0.4021 \left[\frac{O}{C} \right]} \right] LHV_{Biomass}}{\dot{E}_{D,TOTAL}}. \quad (77)$$

3 | Results and Discussions

The results and discussions for thermodynamic simulation of exergy efficiency for different working fluids are presented in this study section. However, considerations were given to standard thermodynamic conventions and performance charts, as well as environmental and safety properties of the operating refrigerants, together with thermodynamic simulations of system parameters as shown.

3.1 | Thermodynamic Assumptions for the Refrigerants Employed in the Simulations

For methodical simulation, the following thermodynamic assumptions were made for the three refrigerants (working fluids) selected.

- I. Ambient temperature of 25°C and pressure of 1.013 bars exit at the inlet to pump after the condenser.
- II. The upper operating pressures for the refrigerants R245fa, R1234yf and R1234ze were respectively 2.500, 3.085 and 3.128 MPa and for lower operating pressures 0.1478, 0.6866 and 0.4959 MPa.
- III. The temperature of the gasifier outlet was at 600°C.
- IV. The pump and turbine isentropic efficiencies were 0.85 each.
- V. The refrigerant mass flow rate was 1.5Kg/s.
- VI. The evaporator pinch point temperature was 40°C.
- VII. The condenser temperature was 35°C.

It should be noted that the thermodynamic assumptions considered were made within the real-time cycle's working boundaries for optimal results.

3.2 | Thermodynamic Performance Tables for Operating Refrigerants

The operating criteria for the plant performance were set considering the physical properties of the refrigerants, as presented in *Table 1*.

Table 1. Physical properties of the operating refrigerants.

Substance	Chemical Formula	Physical Data				
		M(g/mol)	NDP (°C)	T _c (°C)	P _c (MPa)	V _c × 10 ³ (m ³ /Kg)
R245fa	CF ₃ -CH ₂ -CHF ₂	134.05	15.1	154.1	3.65	1.9340
R1234yf	CF ₃ CF=CH ₂	114.04	-29.5	94.7	3.38	0.0021
R1234ze	CHF=CHCF ₃	114.04	-19.0	109.4	3.64	0.0020

3.3 | Environmental and Safety Measurement of the Operating Refrigerant

For environmental and safety indices, the physical properties were presented in *Table 2*.

Table 2. Environmental and safety measurements of the operating refrigerant.

Substance	Chemical Formula	Environmental Data			Safety Data	
		ALT(yr)	ODP (°C)	GWP (100yr)	LFL (%)	Safety Group
R245fa	CF ₃ -CH ₂ -CHF ₂	7.7	0.0	1050	None	B1
R1234yf	CF ₃ CF=CH ₂	0.029	0.0	<1	6.2	A2L
R1234ze	CHF=CHCF ₃	0.045	0.0	<1	7.6	A2L

The selection of working fluid is particularly essential in the performance and modelling of the system since it can accomplish both high performance and minimal environmental issues. Consequently, global warming potential, atmospheric lifetime, Ozone depletion potential, flammability, toxicity, auto ignition, economy and availability were considered. Hence, hydrofluorocarbons have been chosen as working fluids instead of hydrochlorofluorocarbon and chlorofluorocarbons.

3.4 | Thermodynamic Simulations

The results of thermodynamic simulation had values for both intensive and extensive properties of enthalpy, entropy, mass flow rate, exergy and the operating pressures at all state points in the system (plant) cycle, as shown in *Tables 3-5* for R245fa, R1234yf and R1234ze respectively.

Enthalpy is the sum of the internal energy and the product of pressure and volume in a thermodynamic system. It is a thermodynamic property with units in joules but is usually expressed in kilojoules. However, it has other calorie or British Thermal Units (BTUs) units. However, the enthalpy change at constant pressure is exactly heat transfer [33]. Meanwhile, the internal energy of a system is stored energy that results from the random motion of atoms and molecules of a body. It is the sum of microscopic forms of energy that are different from heat energy, which describes the energy transfer process that results from temperature difference [6]. Thermodynamic properties, especially enthalpy, greatly influence the exergy efficiency of ORC since it is a function of pressure and mass flow.

Additionally, entropy, termed the measure of a thermodynamic system's thermal energy per unit temperature that is unavailable for conversion to mechanical work, also affects the efficiency of ORC, and it is temperature dependent [33]. Entropy is often referred to as the degree of disorder or randomness in the system measured in joules per kilogram kelvin but often represented in kilojoules per kilogram kelvin (kJ/kgK) [25].

Table 3. Thermodynamic properties at state points for R245fa.

State	Mass Flow Rate (Kg/s)	P (MPa)	T (°C)	s (KJ/KgK)	h (KJ/KgK)	ex (KW)
1	2.050	2.5000	120	1.511	317.9	56.12
2	1.025	0.7347	77.1	1.511	366.5	22.56
3	1.025	0.1478	25	1.511	351.1	6.772
4	1.025	0.2046	34.11	1.55	366.5	10.7
5	1.025	0.2046	34.11	1.153	244.6	6.98
6	1.025	0.1478	2	1.009	244.6	51
7	1.025	0.1478	2	1.748	405.9	-9.4
8	1.025	0.1478	25	1.339	299.8	6.76
9	2.05	0.1478	25	1.57	352.8	13.54
10	2.05	0.1478	25	1.113	232.5	13.49
11	2.05	2.5	25.8	1.113	234.2	17.08
12	2.05	2.5	45	1.197	259.9	18.87
13	0.2593	0.1013	25	5.695	298.6	0
14	0.04776	0.1013	25	1.38	-9442	896.1
15	0.3071	0.1013	600	19.8	1090	175.6
16	0.0371	0.1013	600	19.8	1090	175.6
17	0.0371	0.1013	85	4.22	342.3	0.7802
18	0.0371	0.1013	65	3.374	313.3	-9442
19	0.08526	0.1013	20	0.2962	83.93	0.01422
20	0.08526	0.1013	45	0.6385	188.5	0.2325

Table 4. Thermodynamic properties at state points for 1234yf.

State	Mass Flow Rate (Kg/s)	P (MPa)	T (°C)	s (KJ/KgK)	h (KJ/KgK)	ex (KW)
1	2.050	3.085	95	1.636	414.4	132.2
2	1.025	2.062	73.73	1.636	408.4	59.92
3	1.025	0.6866	33.29	1.636	388.7	39.7
4	1.025	0.8618	54.63	1.684	408.4	45.2
5	1.025	0.8618	54.63	1.261	279.6	42.35
6	1.025	0.6866	2	1.01	279.6	119.2
7	1.025	0.6866	2	1.599	364.8	26.55
8	1.025	0.6866	25.21	1.438	329.6	39.51
9	2.05	0.6866	25.21	1.497	347.2	79.06
10	2.05	0.6866	25	1.119	234.4	78.78
11	2.05	3.085	26.53	1.126	236.6	78.84
12	2.05	3.085	45	1.241	266.1	85.59
13	0.3435	0.1013	25	5.695	298.6	0
14	0.06326	0.1013	25	1.38	-9442	1187
15	0.4068	0.1013	600	19.8	1090	232.6
16	0.4068	0.1013	600	19.8	1090	232.6
17	0.4068	0.1013	85	4.229	342.3	1.033
18	0.4068	0.1013	65	3.374	313.3	-7.958
19	0.1129	0.1013	20	0.2962	83.93	0.01883
20	0.1129	0.1013	45	0.6385	188.5	0.308

Table 5. Thermodynamic properties at state points for 1234ze.

State	Mass Flow Rate (Kg/s)	P (MPa)	T (°C)	s (KJ/KgK)	h (KJ/KgK)	ex (KW)
1	2.050	2.5000	90	1.391	327	90.26
2	1.025	0.7347	74.15	1.391	325	43.1
3	1.025	0.1478	24.72	1.391	315.3	33.08
4	1.025	0.2046	33.71	1.415	325	35.83
5	1.025	0.2046	33.71	1.148	243.4	33.41
6	1.025	0.4959	2	1.009	243.4	75.98
7	1.025	0.4959	2	1.665	382.9	18.78
8	1.025	0.4959	24.72	1.158	245.9	33.1
9	2.05	0.4959	24.72	1.388	314.4	66.16
10	2.05	0.4959	25	1.662	396.1	66.11
11	2.05	3.128	26.2	1.665	397.1	66.58
12	2.05	3.128	45	1.191	258.9	72.61
13	0.1576	0.1013	25	5.695	298.6	0
14	0.02903	0.1013	25	1.38	-9442	544.7
15	0.1867	0.1013	600	19.8	1090	106.7
16	0.1867	0.1013	600	19.8	1090	106.7
17	0.1867	0.1013	85	4.229	342.3	0.4742
18	0.1867	0.1013	65	3.374	313.3	-3.652
19	0.05182	0.1013	20	0.2962	83.93	0.008642
20	0.05182	0.1013	45	0.6385	188.5	0.1413

From *Tables 3-5* it can be seen that the thermodynamic simulation was carried out on different intrinsic properties for 20 state points, showing the system conditions within the cycle at each instance. For R245fa, the mass flow rate, which determines the input percentage of the working fluid available during operation, varied linearly with fluctuating conditions ranging between 0.0371 – 2.0500 Kg/s and having each cyclic variation after about every 10 state point. Moreover, pressure, another deterministic property of total energy in the system, also had an alternating condition between 0.1013 – 2.5000 MPa with maximum value recorded at the starting state point of the system. Temperature had absolute values ranging from 275 – 873K with entropy varying from 0.2962 – 19.8 kJ/kgK, enthalpy –9442 – 1090 kJ/kgK and exergy output –9442 – 896.1kW. Then, for R1234yf and R1234ze, the respective corresponding values for mass flow rate were 0.06326 – 2.0500 and 0.02903 – 0.0500Kg/s, pressure; 0.1013 – 3.085 and 0.1013 – 3.128 MPa, temperature; 275 – 873K (the same for both), entropy; 0.2962 – 19.8 kJ/kgK (same for both), enthalpy; –9442 – 1090 kJ/kgK (same for both) and exergy output; –7.958 – 1187kW and –3.652 – 544.7kW. It should be noted that the system's absolute temperature, entropy and enthalpy were within the same operating limit for the three refrigerants. The enhanced exergy output of the system was credited to the increase in enthalpy and the system's internal energy due to optimized operating pressure and stabilized discharge of the working fluid [26], [44]. The condition indicates that a high mass flow rate supports high exergy output. Since enthalpy is a function of pressure, therefore high pressure also supports improved exergy efficiency as a result of exergy dependent on enthalpy and internal energy, which aligns with the positions of others [4], [9], [12]-[14]. It also portrays that temperature is a deterministic factor because increased entropy militated against improved exergy efficiency, showing that lower cycle temperature is recommended for improved exergy output [38]. Furthermore, the *Tables* under consideration illustrate that R1234yf had the highest efficiency, then R235fa followed by R1234ze.

3.5 | Cycle Performance at Standard Conditions

The operating conditions analyzed under cycle performance at standard conditions included exergy efficiency, net power output, refrigeration output, the exergy of refrigeration, SI, TIT and heating output, as summarized in *Table 6*.

Table 6. Performance of the system at standard conditions.

Working Fluid	Exergy Efficiency (%)		Net Power Output (KW)	Refrig. Output (KW)	Exergy of Refrig.	SI	TIT (°C)	Heating Output (KW)
	With Cooling	Without Cooling						
R245fa	28.34	15.33	26.80	165.3	13.8	0.8928	120	8.915
R1234yf	22.32	14.06	32.55	87.35	7.305	0.4484	95	11.81
R1234ze	29.61	13.25	14.08	143.00	11.96	0.8638	90	5.419

For effective comparison, nearly the same operating TITs were used for simulations. Accordingly, R1234ze had the maximum efficiency of 29.61%, followed by R245fa with 28.34% and R1234yf with the least value of 22.32%. Comparatively, the generic ORC cycle with turbine bleeding recorded corresponding efficiencies as 13.25, 15.33 and 14.06%, which is relatively low concerning the ORC without cooling. The marginal exergitic efficiency increase results from the cooling effect by reducing the thermal gradient between hot and cold heat reservoirs. As much as 165.3 kW refrigeration output was achieved by R245fa and R1234ze (143 kW) and R1234yf (87.35 kW). It can be observed from *Table 6* that TIT was selected at minimal pressures to enhance power generation, although pitched at superheated conditions. Therefore, TIT was spread as 120 °C, 95 °C and 90 °C, respectively, for R245fa, R1234yf and R1234ze. However, this low range was selected to facilitate the use of the system for very low thermal applications. Additionally, values for both net power output and heating output had inverse proportionality relation with higher thermal conditions supporting the efficient SI of the system. Generally, the decline in exergy efficiency at higher temperatures is due to reduced heat transfer effectiveness and increased irreversibility. In contrast, heat transfer effectiveness is higher at lower operating temperatures, promoting exergy efficiency.

3.6 | Exergy Destruction

The system's exergy destruction and total power output are presented in *Table 7*. The level of component and exergy destruction severely affects the SI concerning the net expander output of the system. It can be observed that R245fa, R1234yf and R1234ze attained respectively exergy destruction of 225.1, 293.8 l and 188.1 KW and their respective total power output of 201, 131.7 and 162.5 KW.

Table 7. Total exergy destruction and output.

Working Fluid	Total Exergy Destruction (KW)	Total Power Output (KW)
R245fa	225.1	201.0
R1234yf	293.8	131.7
R1234ze	188.1	162.5

The level of exergy destruction in the system seems large due to relatively enormous exergy destruction in the evaporator, which stems from the high-temperature difference between the combusting syngas and the working fluids. Accordingly, the SI is sternly limited to values that are less than unity values. However, since the proximity of actual sustainability values is approximately unity, the system can be operated with R245fa and R1234ze.

3.7 | Exergy Output at Variable Mass Flow Rates for Different Working Fluids

The exergy output at variable mass flow rates for the selected working fluids is presented in *Figs. 2-4*, and a comparative analysis is illustrated in *Fig. 5*. The mass flow rate dramatically influences the exergy efficiency of the system as it determines the input parameters that the system takes up at any time. The amount of compressed working fluid per unit of time defines the quantity of combusting syngas at each state during the thermodynamic cycle. It can be observed in *Fig. 2* that exergy output had a fluctuating relationship, recording its maximum value as 56 KW at 0.18 Kg/s mass flow rate. This implies that the marginal input for the working fluid using R245fa refrigerant should be kept within this range for optimal efficiency.

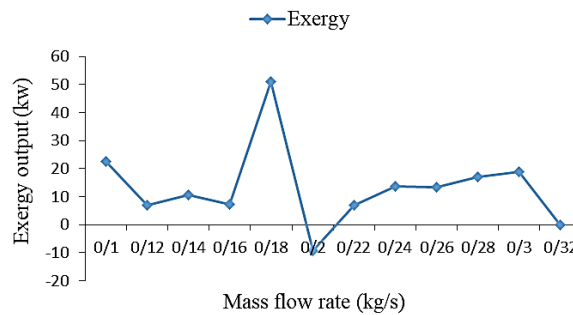


Fig. 2. Effect of mass flow rate on exergy efficiency for R245fa.

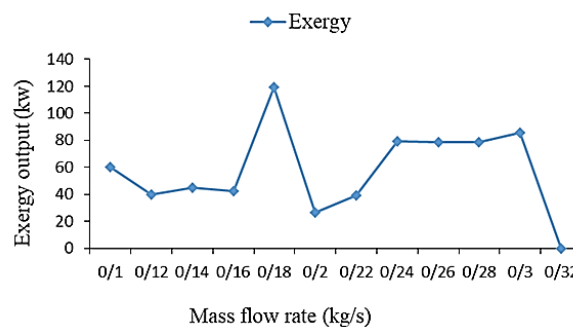


Fig. 3. Effect of mass flow rate on exergy efficiency for R1234yf.

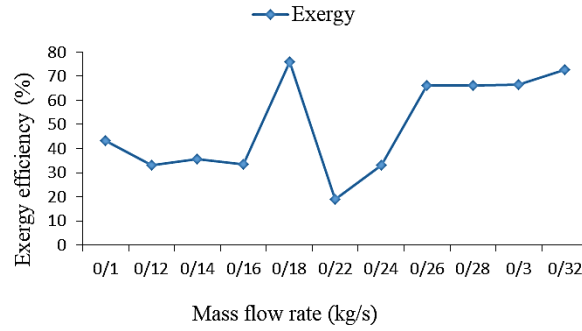


Fig. 4. Effect of mass flow rate on exergy efficiency for R1234ze.

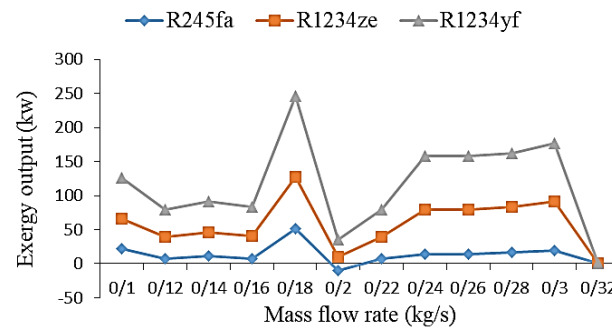


Fig. 5. Comparative analysis of exergy output against mass flow rates for the selected working fluids.

Moreover, for the same mass flow rate, R1234yf and R1234ze, respectively, reached 122 and 79 KW as their maximum exergy output (Fig. 3 and Fig. 4). Fig. 5, which presents the comparative analysis of the three selected working fluids, shows that they all followed the same graphical curve with R1234yf followed by R1234ze and R245fa in that order. This illustrates the baseline operating input rate for overall exergy efficiency.

3.8 | Effect of Mass Flow Rate on System Enthalpy and Pressure

Figs. 6-8 analyse the effect of mass flow rate on enthalpy and operating pressure of the system. Enthalpy determines the valuable energy in a thermodynamic system to be converted to mechanical work. Therefore, higher enthalpy is advantageous. Furthermore, pressure and volumetric efficiency also vary directly, as the system's enthalpy shows that higher pressure and volumetric efficiency favour optimal enthalpy, hence the exergy efficiency of the ORC system. The maximum enthalpies for the working fluids were 395, 400, and 403 KJ/Kg for R245fa, R1234yf and R1234ze respectively attained between the mass flow rate of 0.26-0.32 kg/s. The corresponding operating pressures for all the selected working fluids varied between 1.5-2.5 MPa.

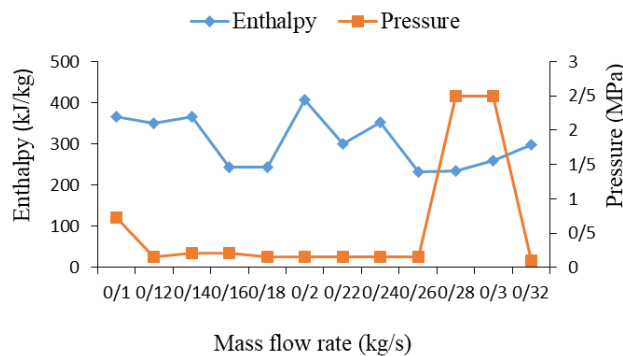


Fig. 6. Effect of mass flow rates on system enthalpy and state pressure (R 234fa).

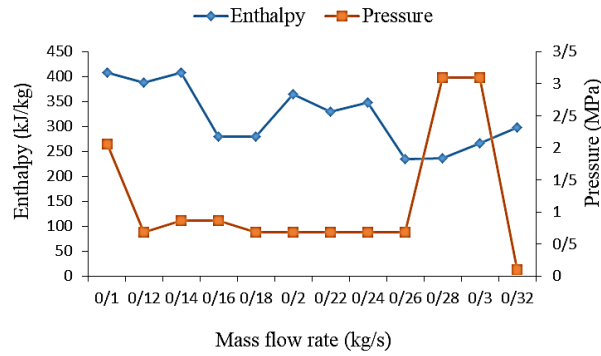


Fig. 7. Effect of mass flow rates on system enthalpy and state pressure (R 1234ze).

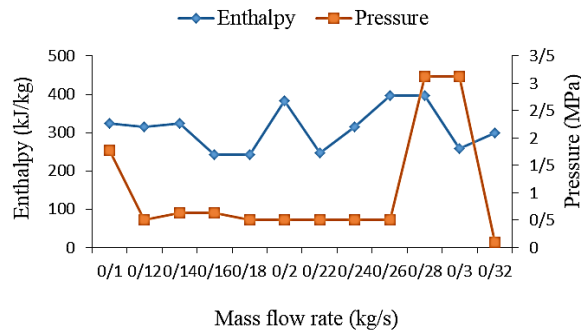


Fig. 8. Effect of mass flow rates on system enthalpy and state pressure (R 1234ze).

3.9 | Effect of Turbine Inlet Pressure on Exergy Efficiency and Turbine Output

The effect of turbine inlet pressure on turbine output and exergy efficiency at base conditions is presented in *Figs. 9-11* increasing turbine inlet pressure at constant turbine back pressure creates a higher pressure gradient, increasing fluid expansion. This, in turn, results in higher turbine output for the three refrigerants. Additionally, with constant heat interaction in the system's evaporator, a larger pressure gradient will increase exergetic efficiencies. The increase in variation in exergy efficiency is linearly related to the configuration of the system in the generation of products. The trend is shown for R245fa and R1234ze where turbine work and exergetic efficiencies increased in tandem with turbine inlet pressures. However, in *Fig. 10*, increasing turbine pressures above certain limits truncates the output. This scenario is particularly observed in R1234yf at pressures within the neighbourhood of the refrigerant's critical pressures. The maximum exergetic efficiencies recorded by R245fa, R1234yf and R1234ze were 28.3, 23.9 and 29.8%, respectively.

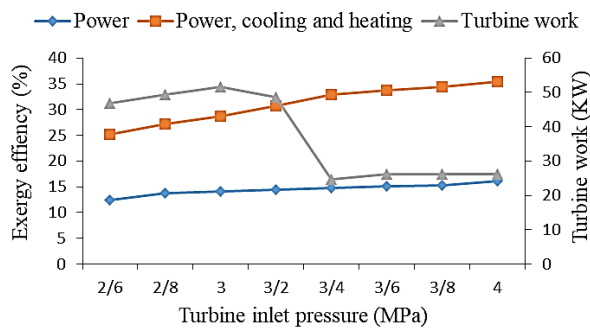


Fig. 9. Effect of varying turbine inlet pressure on exergy efficiency and turbine work (R123fa).

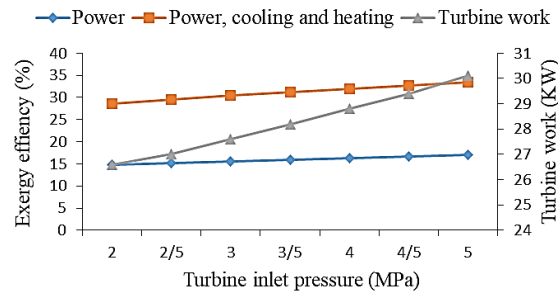


Fig. 10. Effect of varying turbine inlet pressure on exergy efficiency and turbine work (R1234yf).

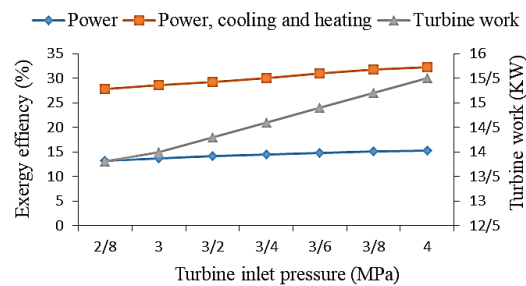


Fig. 11. Effect of varying turbine inlet pressure on exergy efficiency and turbine work (R1234ze).

4 | Conclusion

From the above analysis, there are different sources for powering energy conversion systems operating on ORC and based on the considered fundamental outputs in terms of work, power and trigeneration, R234fa is recommended (preferred), having had the highest overall (combined) efficiency, followed by 1234ze then 1234yf with the least. Moreso, exergy efficiencies for R1234ze, R245fa and R1234yf were recorded as 29.61%, 28.34% and 22.32%, respectively, whereas for the generic ORC without turbine bleeding, with the same configuration had corresponding respective efficiencies of 13.25%, 15.33% and 14.06% which were relatively low with respect to ORC system without cooling, having respective efficiency improvement of 16.36%, 13.0% and 8.26%. Additionally, total output power as 201.0KW for R245fa, 162.5 KW for R1243ze and 131.7 KW for R1234yf with corresponding refrigeration output of 165.3 KW, 87.35 KW and 87.5 KW, respectively. TITs were spread as 120°C, 95°C and 90°C respectively, for R245fa, R1234yf and R1234ze, while SI nearly approached unity (1), especially with R245fa and R1234ze.

As recommendations, the designed ORC system has the potential for medium temperature relevance with agricultural wastes and biomass energy utilisation with reduced vent gases compared to most ORC systems used for low-grade heat sources such as geothermal and solar applications, which are wasted as thermal pollution.

References

- [1] Hall, C. A. S., & Klitgaard, K. (2018). *Energy and the wealth of nations: An introduction to biophysical economics*. Springer Cham. <https://doi.org/10.1007/978-3-319-66219-0>
- [2] Sayigh, A. (2012). *Comprehensive renewable energy*. Elsevier. <https://B2n.ir/n66421>
- [3] Zabihian, F. (2021). *Power plant engineering*. CRC Press. <https://doi.org/10.1201/9780429069451>
- [4] Al-Sulaiman, F. A., Dincer, I., & Hamdullahpur, F. (2010). Exergy analysis of an integrated solid oxide fuel cell and organic Rankine cycle for cooling, heating and power production. *Journal of power sources*, 195(8), 2346–2354. <https://doi.org/10.1016/j.jpowsour.2009.10.075>

- [5] Safarian, S., & Aramoun, F. (2015). Energy and exergy assessments of modified organic Rankine cycles (ORCs). *Energy reports*, 1, 1–7. <https://doi.org/10.1016/j.egy.2014.10.003>
- [6] Eastop, T. D., & Mc Conkey, A. (1986). *Applied thermodynamics for engineering technologies*. John Wiley and Sons Inc. <https://B2n.ir/e82912>
- [7] Oyedepo, S. O. (2012). Energy and sustainable development in Nigeria: the way forward. *Energy, sustainability and society*, 2(15), 1–17. <https://doi.org/10.1186/2192-0567-2-15>
- [8] Rayner, J. (2008). *Basic engineering thermodynamics*. Pearson India. <https://B2n.ir/t74137>
- [9] Ahmadi, P., Dincer, I., & Rosen, M. A. (2013). Thermodynamic modeling and multi-objective evolutionary-based optimization of a new multigeneration energy system. *Energy conversion and management*, 76, 282–300. <https://doi.org/10.1016/j.enconman.2013.07.049>
- [10] Bombarda, P., Invernizzi, C. M., & Pietra, C. (2010). Heat recovery from Diesel engines: A thermodynamic comparison between Kalina and ORC cycles. *Applied thermal engineering*, 30(2), 212–219. <https://doi.org/10.1016/j.applthermaleng.2009.08.006>
- [11] Muñoz De Escalona, J. M., Sánchez, D., Chacartegui, R., & Sánchez, T. (2012). Part-load analysis of gas turbine & ORC combined cycles. *Applied thermal engineering*, 36(1), 63–72. <https://doi.org/10.1016/j.applthermaleng.2011.11.068>
- [12] Zhang, X., Cao, M., Yang, X., Guo, H., & Wang, J. (2019). Economic analysis of organic Rankine cycle using R123 and R245fa as working fluids and a demonstration project report. *Applied sciences (Switzerland)*, 9(2), 288. <https://doi.org/10.3390/app9020288>
- [13] Özdemir Küçük, E., & Kılıç, M. (2023). Exergoeconomic analysis and multi-objective optimization of ORC configurations via Taguchi-Grey Relational methods. *Heliyon*, 9(4). <https://doi.org/10.1016/j.heliyon.2023.e15007>
- [14] Sun, J., Liu, Q., & Duan, Y. (2018). Effects of evaporator pinch point temperature difference on thermo-economic performance of geothermal organic Rankine cycle systems. *Geothermics*, 75, 249–258. <https://doi.org/10.1016/j.geothermics.2018.06.001>
- [15] Wei, D., Lu, X., Lu, Z., & Gu, J. (2008). Dynamic modeling and simulation of an organic Rankine cycle (ORC) system for waste heat recovery. *Applied thermal engineering*, 28(10), 1216–1224. <https://doi.org/10.1016/j.applthermaleng.2007.07.019>
- [16] Li, W., Feng, X., Yu, L. J., & Xu, J. (2011). Effects of evaporating temperature and internal heat exchanger on organic Rankine cycle. *Applied thermal engineering*, 31(17), 4014–4023. <https://doi.org/10.1016/j.applthermaleng.2011.08.003>
- [17] Zhang, Z., Yuan, H., Yi, S., Sun, Y., Peng, W., & Mei, N. (2024). Theoretical analysis on temperature-lifting cycle for ocean thermal energy conversion. *Energy conversion and management*, 300, 117946. <https://doi.org/10.1016/j.enconman.2023.117946>
- [18] Quoilin, S., Orosz, M., Hemond, H., & Lemort, V. (2011). Performance and design optimization of a low-cost solar organic Rankine cycle for remote power generation. *Solar energy*, 85(5), 955–966. <https://doi.org/10.1016/j.solener.2011.02.010>
- [19] Bao, J. J., Zhao, L., & Zhang, W. Z. (2011). A novel auto-cascade low-temperature solar Rankine cycle system for power generation. *Solar energy*, 85(11), 2710–2719. <https://doi.org/10.1016/j.solener.2011.08.015>
- [20] Jin, Y., Gao, N., & Wang, T. (2020). Influence of heat exchanger pinch point on the control strategy of organic Rankine cycle (ORC). *Energy*, 207, 118196. <https://doi.org/10.1016/j.energy.2020.118196>
- [21] Desai, N. B., & Bandyopadhyay, S. (2009). Process integration of organic Rankine cycle. *Energy*, 34(10), 1674–1686. <https://doi.org/10.1016/j.energy.2009.04.037>
- [22] Lu, P., Liang, Zh., Luo, X., Xia, Y., Wang, J., Chen, K., Liang, Y., Chen, J., Yang, Zh., He, J & Chen, Y. (2023). Design and optimization of organic Rankine cycle based on heat transfer enhancement and novel heat exchanger: a review. *Energies*, 16(3), 1380. <https://doi.org/10.3390/en16031380>
- [23] Fallah, M., Mahmoudi, S. M. S., Yari, M., & Akbarpour Ghiasi, R. (2016). Advanced exergy analysis of the Kalina cycle applied for low temperature enhanced geothermal system. *Energy conversion and management*, 108, 190–201. <https://doi.org/10.1016/j.enconman.2015.11.017>
- [24] Kotas, T. J. (2012). *The exergy method of thermal plant analysis*. Paragon publishing.

- [25] Moran, M. J., Shapiro, H. N., Boettner, D. D., & Bailey, M. B. (2010). *Fundamentals of engineering thermodynamics*. John Wiley & Sons. <https://B2n.ir/m11094>
- [26] Long, R., Bao, Y. J., Huang, X. M., & Liu, W. (2014). Exergy analysis and working fluid selection of organic Rankine cycle for low grade waste heat recovery. *Energy*, 73, 475–483. <https://doi.org/10.1016/j.energy.2014.06.040>
- [27] Xu, C., Wang, Z., Li, X., & Sun, F. (2011). Energy and exergy analysis of solar power tower plants. *Applied thermal engineering*, 31(17), 3904–3913. <https://doi.org/10.1016/j.applthermaleng.2011.07.038>
- [28] Dai, Y., Wang, J., & Gao, L. (2009). Parametric optimization and comparative study of organic Rankine cycle (ORC) for low grade waste heat recovery. *Energy conversion and management*, 50(3), 576–582. <https://doi.org/10.1016/j.enconman.2008.10.018>
- [29] Regulagadda, P., Dincer, I., & Naterer, G. F. (2010). Exergy analysis of a thermal power plant with measured boiler and turbine losses. *Applied thermal engineering*, 30(8–9), 970–976. <https://doi.org/10.1016/j.applthermaleng.2010.01.008>
- [30] Aljundi, I. H. (2009). Energy and exergy analysis of a steam power plant in Jordan. *Applied thermal engineering*, 29(2), 324–328. <https://doi.org/10.1016/j.applthermaleng.2008.02.029>
- [31] Gutiérrez, A. S., Martínez, J. B. C., & Vandecasteele, C. (2013). Energy and exergy assessments of a lime shaft kiln. *Applied thermal engineering*, 51(1), 273–280. <https://doi.org/10.1016/j.applthermaleng.2012.07.013>
- [32] Rajput, R. K. (2008). *Heat and Mass Transfer*. Chand (S.) & Co Ltd. <https://B2n.ir/x61529>
- [33] Cengel, Y. A., Boles, M. A., & Kanoğlu, M. (2011). *Thermodynamics: An engineering approach*. McGraw-hill New York.
- [34] Ikpe, A. E., Iluobe, I. C., & Imonitie, D. I. (2020). Modelling and simulation of high pressure fogging air intake cooling unit of omotosho phase II gas turbine power plant. *Journal of applied research on industrial engineering*, 7(2), 121–136. http://www.journal-aprie.com/article_106397.html
- [35] Kuo, C. R., Hsu, S. W., Chang, K. H., & Wang, C. C. (2011). Analysis of a 50kW organic Rankine cycle system. *Energy*, 36(10), 5877–5885. <https://doi.org/10.1016/j.energy.2011.08.035>
- [36] Hung, T. C. (2001). Waste heat recovery of organic Rankine cycle using dry fluids. *Energy conversion and management*, 42(5), 539–553. [https://doi.org/10.1016/S0196-8904\(00\)00081-9](https://doi.org/10.1016/S0196-8904(00)00081-9)
- [37] Tchanche, B. F., Lambrinos, G., Frangoudakis, A., & Papadakis, G. (2011). Low-grade heat conversion into power using organic Rankine cycles - a review of various applications. *Renewable and sustainable energy reviews*, 15(8), 3963–3979. <https://doi.org/10.1016/j.rser.2011.07.024>
- [38] Yamamoto, T., Furuhashi, T., Arai, N., & Mori, K. (2001). Design and testing of the organic Rankine cycle. *Energy*, 26(3), 239–251. [https://doi.org/10.1016/S0360-5442\(00\)00063-3](https://doi.org/10.1016/S0360-5442(00)00063-3)
- [39] Maizza, V., & Maizza, A. (2001). Unconventional working fluids in organic Rankine-cycles for waste energy recovery systems. *Applied thermal engineering*, 21(3), 381–390. [https://doi.org/10.1016/S1359-4311\(00\)00044-2](https://doi.org/10.1016/S1359-4311(00)00044-2)
- [40] Badr, O., O’Callaghan, P. W., & Probert, S. D. (1990). Rankine-cycle systems for harnessing power from low-grade energy sources. *Applied energy*, 36(4), 263–292. [https://doi.org/10.1016/0306-2619\(90\)90002-U](https://doi.org/10.1016/0306-2619(90)90002-U)
- [41] Chen, H., Goswami, D. Y., & Stefanakos, E. K. (2010). A review of thermodynamic cycles and working fluids for the conversion of low-grade heat. *Renewable and sustainable energy reviews*, 14(9), 3059–3067. <https://doi.org/10.1016/j.rser.2010.07.006>
- [42] Zhao, W., Xie, N., Zhang, W., Yue, J., Wang, L., Bu, X., & Li, H. (2021). Performance characteristics and working fluid selection for high-temperature organic Rankine cycle driven by solar parabolic trough collector. *International journal of low-carbon technologies*, 16(4), 1135–1149. <https://doi.org/10.1093/ijlct/ctab036>
- [43] Soltani, S., Mahmoudi, S. M. S., Yari, M., & Rosen, M. A. (2013). Thermodynamic analyses of an externally fired gas turbine combined cycle integrated with a biomass gasification plant. *Energy conversion and management*, 70, 107–115. <https://doi.org/10.1016/j.enconman.2013.03.002>
- [44] Cohce, M. K., Dincer, I., & Rosen, M. A. (2011). Energy and exergy analyses of a biomass-based hydrogen production system. *Bioresource technology*, 102(18), 8466–8474. <https://doi.org/10.1016/j.biortech.2011.06.020>

- [45] Ahmadi, P., Dincer, I., & Rosen, M. A. (2013). Development and assessment of an integrated biomass-based multi-generation energy system. *Energy*, 56, 155–166. <https://doi.org/10.1016/j.energy.2013.04.024>
- [46] Koroneos, C., & Lykidou, S. (2011). Equilibrium modeling for a downdraft biomass gasifier for cotton stalks biomass in comparison with experimental data. *Journal of chemical engineering and materials science*, 2(4), 61–68. <https://B2n.ir/m24659>
- [47] Nafey, A. S., Sharaf, M. A., & García-Rodríguez, L. (2010). Thermo-economic analysis of a combined solar organic Rankine cycle-reverse osmosis desalination process with different energy recovery configurations. *Desalination*, 261(1), 138–147. <https://doi.org/10.1016/j.desal.2010.05.017>
- [48] Zahedi, R., Ahmadi, A., & Dashti, R. (2021). Energy, exergy, exergoeconomic and exergoenvironmental analysis and optimization of quadruple combined solar, biogas, SRC and ORC cycles with methane system. *Renewable and sustainable energy reviews*, 150, 111420. <https://doi.org/10.1016/j.rser.2021.111420>
- [49] Jouhara, H., Khordehghah, N., Almahmoud, S., Delpech, B., Chauhan, A., & Tassou, S. A. (2018). Waste heat recovery technologies and applications. *Thermal science and engineering progress*, 6, 268–289. <https://doi.org/10.1016/j.tsep.2018.04.017>
- [50] Wang, L., Guo, Y., Liu, K., Wang, C., Che, D., Yang, X., & Sundén, B. (2023). Numerical study on dynamic performance of low temperature recuperator in a S-CO₂ Brayton cycle. *Numerical heat transfer; part a: applications*, 84(12), 1436–1458. <https://doi.org/10.1080/10407782.2023.2176382>
- [51] Li, X., Song, J., Yu, G., Liang, Y., Tian, H., Shu, G., & Markides, C. N. (2019). Organic Rankine cycle systems for engine waste-heat recovery: heat exchanger design in space-constrained applications. *Energy conversion and management*, 199, 111968. <https://doi.org/10.1016/j.enconman.2019.111968>
- [52] kaşka, ö. (2014). Energy and exergy analysis of an organic Rankine for power generation from waste heat recovery in steel industry. *energy conversion and management*, 77, 108–117. <https://doi.org/10.1016/j.enconman.2013.09.026>
- [53] Baroutaji, A., Arjunan, A., Ramadan, M., Robinson, J., Alaswad, A., Abdelkareem, M. A., & Olabi, A. G. (2021). Advancements and prospects of thermal management and waste heat recovery of PEMFC. *International journal of thermofluids*, 9, 100064. <https://doi.org/10.1016/j.ijft.2021.100064>
- [54] Poljak, I. (2022). Marine power systems. *Journal of marine science and engineering*, 10(2), 195. <https://doi.org/10.3390/jmse10020195>
- [55] Karellas, S., Schuster, A., & Leontaritis, A. D. (2012). Influence of supercritical ORC parameters on plate heat exchanger design. *Applied thermal engineering*, 33, 70–76. <https://doi.org/10.1016/j.applthermaleng.2011.09.013>
- [56] Laouid, Y. A. A., Kezrane, C., Lasbet, Y., & Pesyridis, A. (2021). Towards improvement of waste heat recovery systems: A multi-objective optimization of different organic Rankine cycle configurations. *International journal of thermofluids*, 11, 100100. <https://doi.org/10.1016/j.ijft.2021.100100>
- [57] Mago, P. J., Chamra, L. M., Srinivasan, K., & Somayaji, C. (2008). An examination of regenerative organic Rankine cycles using dry fluids. *Applied thermal engineering*, 28(8), 998–1007. <https://doi.org/10.1016/j.applthermaleng.2007.06.025>
- [58] Hajabdollahi, H., Ganjehkaviri, A., & Mohd Jaafar, M. N. (2015). Thermo-economic optimization of RSORC (regenerative solar organic Rankine cycle) considering hourly analysis. *Energy*, 87, 369–380. <https://doi.org/10.1016/j.energy.2015.04.113>
- [59] Wang, X., Rahman, Z. U., Lv, Z., Zhu, Y., Ruan, R., Deng, Sh., Zhang, L., & Tan, H. (2021). Experimental study and design of biomass co-firing in a full-scale coal-fired furnace with storage pulverizing system. *Agronomy*, 11(4), 810. <https://doi.org/10.3390/agronomy11040810>
- [60] Darvish, K., Ehyaei, M. A., Atabi, F., & Rosen, M. A. (2015). Selection of optimum working fluid for organic Rankine cycles by exergy and exergy-economic analyses. *Sustainability (Switzerland)*, 7(11), 15362–15383. <https://doi.org/10.3390/su71115362>
- [61] Roy, J. P., & Misra, A. (2012). Parametric optimization and performance analysis of a regenerative organic Rankine cycle using R-123 for waste heat recovery. *Energy*, 39(1), 227–235. <https://doi.org/10.1016/j.energy.2012.01.026>

- [62] Imran, M., Park, B. S., Kim, H. J., Lee, D. H., Usman, M., & Heo, M. (2014). Thermo-economic optimization of regenerative organic Rankine cycle for waste heat recovery applications. *Energy conversion and management*, 87, 107–118. <https://doi.org/10.1016/j.enconman.2014.06.091>
- [63] Bernardoni, C., Binotti, M., & Giostri, A. (2019). Techno-economic analysis of closed OTEC cycles for power generation. *Renewable energy*, 132, 1018–1033. <https://doi.org/10.1016/j.renene.2018.08.007>
- [64] Kasaeian, A., Mirjavadi, K., Pourmoghadam, P., Asgari Sima, F., Amirhaeri, Y., Borhani, S., & Fereidooni, L. (2022). Organic Rankine cycles powered by parabolic trough collectors: an overview. *Sustainable energy technologies and assessments*, 54, 102847. <https://doi.org/10.1016/j.seta.2022.102847>
- [65] Siddiqui, M. E., Almatrafi, E., & Saeed, U. (2023). Performance analysis of organic Rankine cycle with internal heat regeneration: comparative study of binary mixtures and pure constituents in warm regions. *Processes*, 11(8), 2267. <https://doi.org/10.3390/pr11082267>
- [66] Elahi, A. E., Mahmud, T., Alam, M., Hossain, J., & Biswas, B. N. (2022). Exergy analysis of organic Rankine cycle for waste heat recovery using low GWP refrigerants. *International journal of thermofluids*, 16, 100243. <https://doi.org/10.1016/j.ijft.2022.100243>
- [67] Hughes, E. E., & Tillman, D. A. (1998). Biomass cofiring: status and prospects 1996. *Fuel processing technology*, 54(1–3), 127–142. [https://doi.org/10.1016/S0378-3820\(97\)00064-7](https://doi.org/10.1016/S0378-3820(97)00064-7)
- [68] Balaji, C. (2021). *Thermal system design and optimization*. Springer Cham. <https://doi.org/10.1007/978-3-030-59046-8>
- [69] Ahmadi, P., Dincer, I., & Rosen, M. A. (2012). Exergo-environmental analysis of an integrated organic Rankine cycle for trigeneration. *Energy conversion and management*, 64, 447–453. <https://doi.org/10.1016/j.enconman.2012.06.001>
- [70] Liu, H., Shao, Y., & Li, J. (2011). A biomass-fired micro-scale CHP system with organic Rankine cycle (ORC)-thermodynamic modelling studies. *Biomass and bioenergy*, 35(9), 3985–3994. <https://doi.org/10.1016/j.biombioe.2011.06.025>